Cubic lead perovskite PbMoO$_3$ with anomalous metallic behavior

Hiroshi Takatsu,[1] Olivier Hernandez,[2] Wataru Yoshimune,[1] Carmelo Prestipino,[2] Takafumi Yamamoto,[1] Cedric Tassel,[1] Yoji Kobayashi,[1] Dmitry Batuk,[3] Yuki Shibata,[1] Artem M. Abakumov,[3,4] Craig M. Brown,[5] and Hiroshi Kageyama[1]

[1]*Department of Energy and Hydrocarbon Chemistry, Graduate School of Engineering, Kyoto University, Kyoto 615-8510, Japan*

[2]*Institut des Sciences Chimiques de Rennes, UMR CNRS 6226, Université de Rennes 1, Bâtiment 10B, Campus de Beaulieu, Rennes F-35042, France*

[3]*EMAT, University of Antwerp, 2020 Antwerpen, Belgium*

[4]*Skolkovo Institute of Science and Technology, Nobel straße 3, 143026 Moscow, Russia*

[5]*National Institute of Standards and Technology, Center for Neutron Research Gaithersburg, Maryland 20899-6102, USA*

A previously unreported Pb-based perovskite PbMoO$_3$ is obtained by high-pressure and high-temperature synthesis. This material crystallizes in the $Pm\bar{3}m$ cubic structure at room temperature, making it distinct from typical Pb-based perovskite oxides with a structural distortion. PbMoO$_3$ exhibits a metallic behavior down to 0.1 K with an unusual T-sublinear dependence of the electrical resistivity. Moreover, a large specific heat is observed at low temperatures accompanied by a peak in C_P/T^3 around 10 K, in marked contrast to the isostructural metallic system SrMoO$_3$. These transport and thermal properties for PbMoO$_3$, taking into account anomalously large Pb atomic displacements detected through diffraction experiments, are attributed to a low-energy vibrational mode, associated with incoherent off-centering of lone-pair Pb^{2+} cations. We discuss the unusual behavior of the electrical resistivity in terms of a polaronlike conduction, mediated by the strong coupling between conduction electrons and optical phonons of the local low-energy vibrational mode.

I. INTRODUCTION

Insulating oxides with a stereochemically active lone pair of Pb^{2+} and Bi^{3+} cations have been the subject of long-standing interest due to large remnant polarization and high-temperature structural/electronic transitions, as found in Pb(Zr,Ti)O$_3$ with a coherent displacement of Zr/Ti atoms [1,2]. A surge of interest in multiferroics over the last decade has led to numerous studies of BiFeO$_3$ [3] targeting applications in ferroelectric nonvolatile memory devices with high working temperature. More recently, there has been growing interest in ferroelectriclike structural distortion or transition in metallic compounds [4–8]. This is because unprecedented behaviors can appear distinct from conventional metals, such as an enhanced thermoelectric property in (Mo,Nb)Te$_2$ [6] and possible odd-parity superconductivity proposed in Cd$_2$Re$_2$O$_7$ and doped SrTiO$_3$ heterostructures [7].

The concept of introducing polar distortion in a metallic phase has been recently demonstrated in a material of the LiNbO$_3$-structure type, LiOsO$_3$ [8]. It is discussed that large thermal vibration or incoherent disorder of Li and O ions allows cooperative order upon cooling. A ferroelectric-type structural phase transition occurs at $T_s = 140$ K, where the metallic conduction associated with Os half-filled t_{2g} states is retained across T_s. In this context, compounds with stereochemically active lone-pair electrons can be considered as an alternative path for designing ferroelectriclike metal or a new class of metal, since the lone-pair electrons may promote a certain structural distortion [9,10]. However, the research seeking for novel properties from metallic materials with Pb^{2+} or Bi^{3+} cations is rather limited [11–13].

In this paper, we report the synthesis of a Pb-based perovskite PbMoO$_3$ crystallizing in the cubic structure, despite the presence of Pb^{2+} cations. While this material shows an orthorhombic distortion with coherent octahedral tiltings at

low temperature, it retains a metallic behavior down to 0.1 K. We found an unusual temperature dependence of the electrical resistivity ρ and a large specific heat C_P accompanied by a peak in C_P/T^3. These unusual behaviors likely originate from a low-energy vibrational mode induced by the incoherent off-centering of lone-pair Pb^{2+} cations as suggested from structural refinements. The weak T dependence of ρ is presumably understood in terms of incoherent transport driven by the formation of the polaronlike conduction.

II. EXPERIMENT

Polycrystalline samples of Pb$_{1-x}$Sr$_x$MoO$_3$ ($x = 0.0, 0.25, 0.5, 0.75$), were synthesized by a high-pressure and high-temperature technique. Stoichiometric mixtures of PbO, SrO, and MoO$_2$ were reacted at 1000 °C and 7 GPa for 30 min using a multianvil press. SrMoO$_3$ ($x = 1$) was synthesized by heating SrMoO$_4$ (prepared by a solid-state reaction) at 1000 °C for 12 h in H$_2$/Ar flow as reported in Ref. [14].

X-ray powder-diffraction (XRD) experiments were performed with Cu $K\alpha$ radiation at room temperature (RT). For an additional structural study of PbMoO$_3$, synchrotron x-ray powder diffraction (SXRD) experiments were performed at RT on the BL02B2 beam line at SPring-8. The wavelength of the incident beam was $\lambda = 0.42089$ Å. Neutron diffraction experiments of PbMoO$_3$ were performed at RT and 5 K using the high-resolution powder diffractometer BT-1 at the NIST Center for Neutron Research. Incident neutrons of wavelength $\lambda = 1.5398$ Å monochromated by a vertical-focused Cu (311) monochromator were used. The structural refinements were performed using the FULLPROF and RIETAN-FP softwares [15,16]. The $x = 0$ sample was also characterized using transmission electron microscopy (TEM). The data

were acquired on an aberration-corrected FEI Titan 80-300 microscope at 300 kV. The chemical composition was analyzed by energy dispersive x-ray spectroscopy (EDS). The valence was checked by the x-ray absorption near-edge structure (XANES) spectroscopy at the Mo K edge. The spectra of $PbMoO_3$, $SrMoO_3$, MoO_2, and MoO_3 were measured at RT on the BL01B1 beamline at SPring-8. The XANES spectra were recorded in a transmittance mode, using Si (111) and Si (311) double crystal monochromators.

The specific heat (C_P) and dc magnetic susceptibility (M/H) were measured, respectively, with a commercial calorimeter (Quantum Design, PPMS) and a SQUID magnetometer (Quantum Design, MPMS). The electrical resistivity ρ was measured by means of a standard four-probe method using rectangular samples cut out from pellets. Gold wires were attached to samples with silver paste, and the samples were then cooled down to 0.1 K using an adiabatic demagnetization refrigerator installed in PPMS. Note that the density of the polycrystalline sample pellet is 8.7 g/cm^3 for $PbMoO_3$, 7.4 g/cm^3 for $Pb_{0.5}Sr_{0.5}MoO_3$, and 5.4 g/cm^3 for $SrMoO_3$. These values correspond to 89%–97% of the calculated ones estimated from the RT crystal structures, suggesting that the difference in density provides only a small effect on the absolute values of ρ in these compounds.

III. RESULTS AND DISCUSSION

Figure 1 shows the powder SXRD pattern of $PbMoO_3$ recorded at RT. Observed peaks are indexed in a cubic unit cell, without any splitting and shoulder indicating symmetry lowering [see, for example, 211 and 321 reflections in Figs. 1(b) and 1(c)]. This result demonstrates the absence of any distortions from the cubic symmetry at RT. The Rietveld refinement assuming the ideal cubic perovskite (space group: $Pm\bar{3}m$) converged resulting in the lattice parameter of $a = 3.999(1)$ Å and R factors of $R_{wp} = 3.85\%$, $R_e = 3.03\%$, $R_p = 2.99\%$, and $R_B = 3.51\%$. The goodness-of-fit parameter, $S = R_{wp}/R_e$, was $S = 1.27$, indicating excellent quality of the fitting. The solid solution $Pb_{1-x}Sr_xMoO_3$ was successfully obtained in the entire x range, with the lattice constant decreasing linearly with increasing x (Fig. 1 of the Supplemental Material [17]). These results ensure a continuous change in the A-site composition. Refining the occupancy factor of each atomic site did not improve the overall fit, indicating the stoichiometric composition of the title compound at least for the heavy atoms on the A and B sites. The Mo K-edge XANES spectra of $PbMoO_3$ (Fig. 2), measured together with other Mo compounds, indicate that the formal valence in $PbMoO_3$ is Mo^{4+} (thus yielding Pb^{2+}), which is consistent with the result of bond valence sum calculations based on the RT structure, giving Mo$^{4.08+}$ and Pb$^{1.74+}$. EDS experiments verified the compositional ratio between Pb and Mo; for example, Pb/Mo = 1.01(6) for the $x = 0$ sample.

Interestingly, a large atomic displacement parameter (ADP) of Pb was obtained [isotropic root-mean-square displacement of 0.15(1)Å], suggesting unusually large thermal vibration of Pb ions and/or random displacements of Pb away from the ideal position. Given the presence of stereochemically active 6s electrons of Pb^{2+}, the obtained cubic structure in $PbMoO_3$ is unusual and contrasts markedly with other
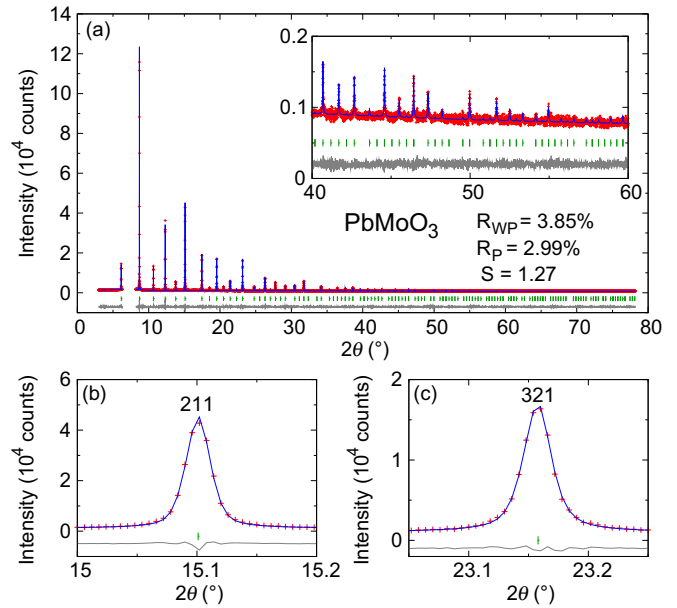

FIG. 1. (a) Synchrotron patterns of $PbMoO_3$ measured at RT, demonstrating the cubic perovskite structure ($Pm\bar{3}m$). The inset shows the enlarged plot in a high-angle region. (b) and (c) are 211 and 321 reflections, respectively, representative peaks with $h \neq k$, $\neq l$, and $l \neq 0$, showing the absence of splitting and shoulder associated with any tetragonal or other symmetry lowering distortions. Observed and refined data are shown by cross and solid curves, and vertical bars represent positions of the Bragg reflections. The difference between the experimental and theoretical data is plotted by the dashed curves at the bottom. Excluded regions in (a) include contributions from small amounts of impurities such as $PbMoO_4$.

reported Pb-based perovskites with a distortion from the cubic symmetry [13]. In order to gain more insight into the RT crystal structure for $PbMoO_3$, we performed TEM experiments. As shown in Figs. 3(a)–3(c), electron-diffraction patterns can be consistently indexed on the cubic perovskite structure with the $Pm\bar{3}m$ symmetry. They do not contain any extra reflections or
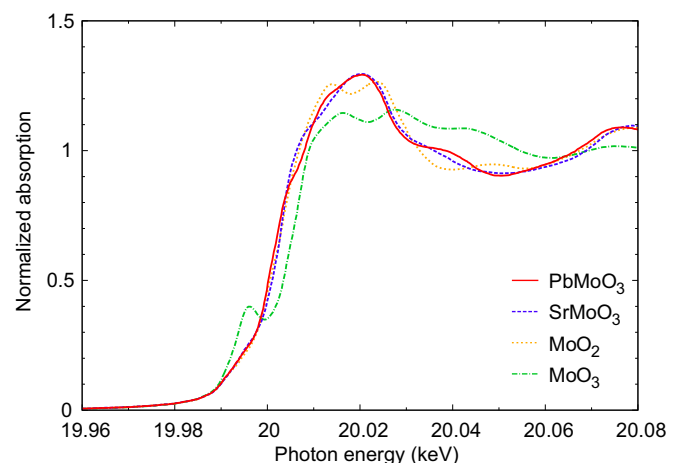

FIG. 2. Mo K-shell XANES spectra of $PbMoO_3$ (solid line), $SrMoO_3$ (dashed line), MoO_2 (dotted line), and MoO_3 (dashed-dotted line).
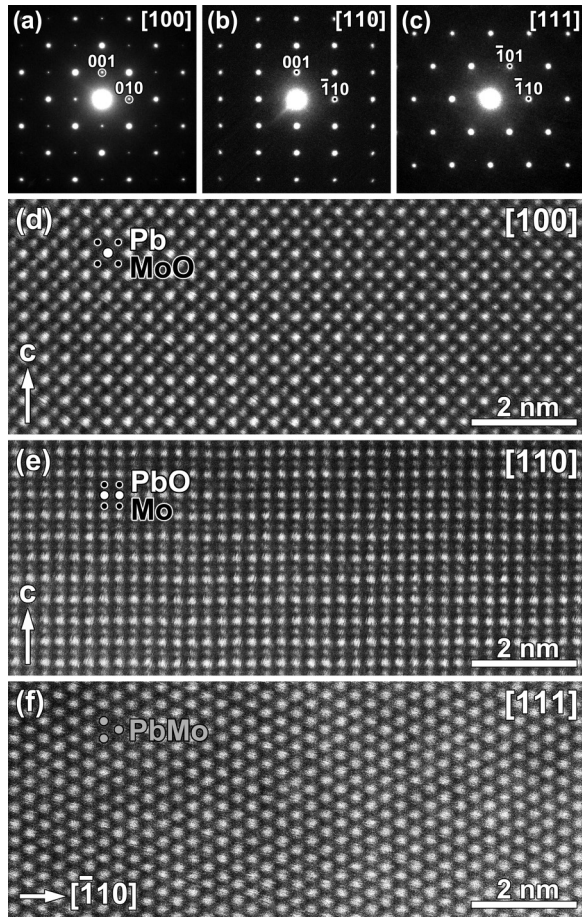
FIG. 3. (a)–(c) Electron-diffraction patterns and (d)–(f) high-resolution HAADF-STEM images of PbMoO$_3$ taken at RT along the [100], [110], and [111] axes. The intensity I in the HAADF-STEM images is proportional to the average atomic number, Z, of the projected atomic column and scales as $I \sim Z^n$ ($n = 1.6$–1.9).

TABLE I. Structure parameters for PbMoO$_3$ refined by Rietveld analysis of the synchrotron x-ray and neutron diffraction data. For each model, the Mo atom was positioned at the origin. U_{iso} represents the isotropic atomic displacement parameter. Numbers in parentheses indicate one standard deviation in the value.

	X-ray (RT)	Neutron (RT)	Neutron (5 K)
Cell parameters and positions			
Space group	$Pm\bar{3}m$	$Pm\bar{3}m$	$Imma$
a (Å)	3.999(3)	3.9986(1)	5.6348(2)
b (Å)			7.9680(3)
c (Å)			5.6508(2)
Pb x	0.5	0.5	0.0
Pb y	0.5	0.5	0.25
Pb z	0.5	0.5	0.5008(17)
O1 x	0.5	0.5	0.0
O1 y	0.0	0.0	0.25
O1 z	0.0	0.0	0.0259(12)
O2 x			0.25
O2 y			$-0.0128(5)$
O2 z			0.25
U_{iso} (10^{-2} Å^2)			
Pb	2.08(6)	2.58(5)	1.2(2)
Mo	0.30(6)	0.64(4)	0.36(4)
O1	0.8(3)	0.99(6)	0.6(2)
O2			0.42(8)

Indeed, a successful structural refinement at 5 K was conducted assuming a low-temperature structural phase analogous to SrMoO$_3$ (space group: $Imma$): details are given in Table I and the Supplemental Material [17]. It is notable that, unlike SrMoO$_3$, the displacement parameter of the Pb site is still quite large even at 5 K (root-mean-square displacement of 0.15 Å along the a axis and ~ 0.08 Å along the b and c axes), suggesting a strong "statically" remaining incoherent Pb off-centering. It is worth underlining that the difference in U_{iso} with T for Pb between RT and 5 K is at least three times higher than that for Mo in PbMoO$_3$ or for Sr in SrMoO$_3$ [22], additionally revealing an unusual thermal behavior possibly related to the dynamic component of lead disorder. We will discuss the effect of the Pb off-centering on physical properties in the next section. As will be shown below, the absence of any anomalies related to the structural transition in C_P, M/H, and ρ may be related to the associated subtle octahedral tilt of about $4°$ along the a axis.

It is expected that the off-centered Pb^{2+} derived from lone-pair electrons in PbMoO$_3$ may provide essential influence on physical properties. In fact, C_P/T of PbMoO$_3$ is much larger than that of SrMoO$_3$ below 150 K. Moreover, the C_P/T^3 vs T plot for PbMoO$_3$ clearly exhibits a peak centered at about 10 K, which is, however, absent in SrMoO$_3$ (see the inset of Fig. 4). This low-temperature peak cannot be explained in terms of the structural phase transition of PbMoO$_3$ and the simple Debye law with $C_P(T) \propto T^3$, and hence implies a significant contribution of a low-energy vibrational mode to the specific heat [23,24]. It is also seen that Sr-for-Pb substitution does not alter the C_P/T^3 peak position (temperature), while reducing only its intensity. It can thus be deduced that this peak originates from the incoherent displacement of Pb ions by the 6s lone-pair

diffuse intensities associated with long- or short-range-ordered structure deformations due to the Pb off-center displacements. Also, high-angle annular dark-field scanning transmission electron microscopy (HAADF-STEM) images in Figs. 3(d)–3(f) do not show any notable discrepancy from the ideal cubic perovskite structure. No anomaly associated with Pb disorder is observed in any principle directions of the cubic structure, [100], [110], and [111]. These results suggest that the Pb off-center displacements, if present, are random at RT, and the local cooperative structure related to correlated disorder [18] or the formation of a polar nanoregion for relaxor phenomena of Pb-based complex perovskites [19–21] is absent.

Rietveld refinement of the RT neutron diffraction data gave a consistent result compared to the SXRD data, confirming the full occupancy of the anionic site, while at $T = 5$ K we found an orthorhombic distortion with additional peaks corresponding to a $\sqrt{2} \times \sqrt{2} \times 2$ cell (Fig. 2 of the Supplemental Material [17]): a preliminary SXRD experiment shows the structural phase transition appears at $T_s \simeq 200$ K. This superstructure is presumably related to a structural transition as observed in SrMoO$_3$ below 125 K involving the softening of a R_{25} phonon mode that results in MoO$_6$ octahedral tilting [22].
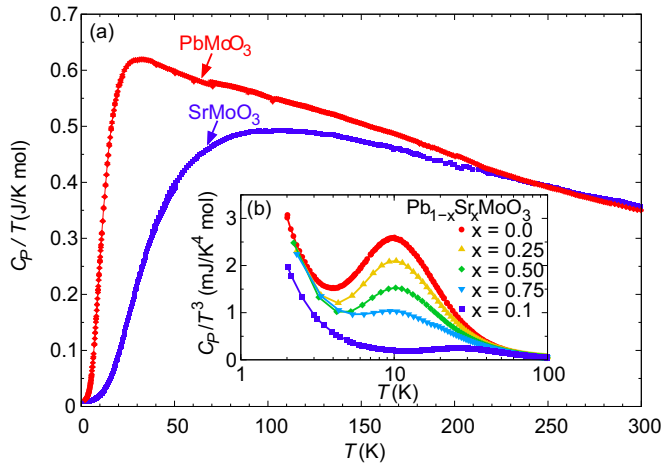
FIG. 4. Temperature dependence of C_P/T for powder samples of PbMoO$_3$ and SrMoO$_3$. A large difference of C_P/T emerges below 150 K, suggesting the contribution of a low-energy vibrational mode in PbMoO$_3$. The inset represents the C_P/T^3 vs T plot for Pb$_{1-x}$Sr$_x$MoO$_3$.

FIG. 5. Temperature dependence of ρ for PbMoO$_3$, Pb$_{0.5}$Sr$_{0.5}$MoO$_3$, and SrMoO$_3$. Here the data for SrMoO$_3$ are multiplied by 10 for clarity. A tiny difference of the data at 0 and 0.5 T below 7 K for PbMoO$_3$ is attributed to a small amount of a Pb impurity which is less than 0.1% examined from diffraction and magnetic susceptibility experiments. Other signatures of SC transition or spin-density wave have not been observed down to 0.1 K in PbMoO$_3$. The inset shows the low-temperature behavior of ρ plotted as a function of $T^{0.5}$ for PbMoO$_3$.

electrons, revealed by the large ADP of Pb, since conventional disorder is known to shift the peak temperature [25–27]. The C_P/T^3 peak for PbMoO$_3$ can be roughly reproduced by the Einstein specific heat with an Einstein temperature $\Theta_E \simeq 50$ K which corresponds to the value estimated from the ADP value of Pb at RT [17]. An upturn of C_P/T^3 observed in Pb$_{1-x}$Sr$_x$MoO$_3$ systems below 5 K is ascribed to the electronic specific heat γT, and we obtained $\gamma = 9.2(1)$ mJ/K^2 mol for PbMoO$_3$ and $\gamma = 7.6(1)$ mJ/K^2 mol for SrMoO$_3$, the latter being in agreement with the previous estimation [28,29]. The Wilson ratio $R_W \equiv \pi^2 k_B^2 \chi_0/(3\mu_B^2 \gamma)$ is obtained as 1.8 and 2.2 for PbMoO$_3$ and SrMoO$_3$, respectively, using the Pauli paramagnetic susceptibility χ_0 after diamagnetic correction for PbMoO$_3$ and χ_0 from the report on SrMoO$_3$ [17,28]. The values of R_W for both compounds are close to 2 as expected in Fermi liquids within the strong correlation limit [30].

The temperature dependence of the electrical resistivity $\rho(T)$ of PbMoO$_3$ (Fig. 5) shows a metallic behavior down to 0.1 K [apart from a tiny contribution of the superconductivity (SC) from the Pb impurity below 7 K]. This SC contribution can be removed by applying a magnetic field of 0.5 T, which is above the critical field of the SC transition of Pb. The resulting $\rho(T)$ is almost identical with the zero-field data, implying that the magnetoresistance is negligible. Interestingly, $\rho(T)$ of PbMoO$_3$ exhibits an unusual T-sublinear dependence in a wide temperature range below 100 K, where the fitting with $\rho(T) = A + BT^\alpha$ to the data yielded $\alpha \simeq 0.5$ (the inset of Fig. 5). Moreover, the resistive change in temperature is rather small, with a residual resistivity ratio RRR $= \rho(300$ K$)/\rho(0.1$ K$) = 1.1$. These features are distinct from $\rho(T)$ of typical nonmagnetic metals, where $\rho(T) \propto T$ or $\propto T^5$ due to the electron-phonon scattering with the weak electron-phonon coupling [31,32] and/or $\rho(T) \propto T^2$ due to the electron-electron scattering are observed at low temperature [33,34]. Note that SrMoO$_3$ shows $\rho(T) \propto T^2$ below 140 K (the main panel of Fig. 5) owing to the enhanced electron-electron correlation [29]. We also observed that $\rho(T) \propto T^2$ is recovered
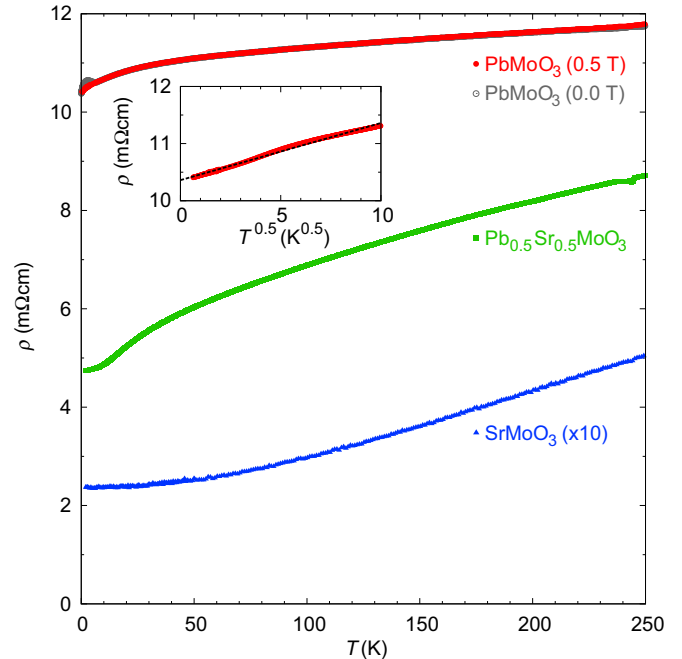
by substituting Pb ions by Sr ions at low temperatures for the $x = 0.5$ sample. Therefore, it appears that incoherent off-centered Pb^{2+} ions disturb the electrical conduction. It is known that a weak coupling between optical phonons and conduction electrons gives rise to a T-superlinear dependence with $\rho(T) \propto T^n$ ($n \geqslant 1$) [32,35]. It is thus possible that the observed polaronlike incoherent transport is mediated by strong coupling between conduction electrons and optical phonons of the local low-energy vibrational mode for PbMoO$_3$, as proposed theoretically by Millis *et al.* [36]. It was suggested that $\rho(T) \propto T^{0.5}$ can appear in the critical regime around the crossover from Fermi liquid to polaron behaviors.

IV. CONCLUSION

To summarize, we have synthesized a lead perovskite PbMoO$_3$ using a high-pressure and high-temperature reaction. This lead-based compound represents a rare case with the $Pm\bar{3}m$ cubic structure at room temperature, despite the presence of Pb^{2+} cations with lone-pair electrons. We observed an unusual T-sublinear dependence in $\rho(T)$ as well as large specific heat at low temperatures, which could be explained in terms of a low-energy vibrational mode mediated by the incoherent off-centering of Pb^{2+} cations as experimentally indicated by anomalously large Pb atomic displacements. Furthermore, the weak T dependence of $\rho(T)$ implies a polaronlike conduction, mediated by the

strong trapping of conduction electrons by local phonon vibration.

Note added. Recently, we became aware of the work on Pb$_2$Cr$_{1+x}$Mo$_{1-x}$O$_6$ reporting a synthesis for $x = -1, -2/3, -1/3, 0, 1/3$ ($x = -1$ means PbMoO$_3$), yet with no structural refinement (thus no indication of Pb off-centering) or detailed physical properties [37].

[1] N. Setter and E. L. Cross, *Ferroelectric Ceramics* (Birkhauser Verlag AG, Basel, 1993).

[2] B. Jaffe, W. R. Cook, and H. Jaffe, *Piezoelectric Ceramics* (Elsevier Science & Technology, New York, 1971).

[3] J. Wang, J. B. Neaton, H. Zheng, V. Nagarajan, S. B. Ogale, B. Liu, D. Viehland, V. Vaithyanathan, D. G. S. U. V. Waghmare, N. A. Spaldin *et al.*, Science **299**, 1719 (2003).

[4] P. W. Anderson and E. I. Blount, Phys. Rev. Lett. **14**, 217 (1965).

[5] I. A. Sergienko, V. Keppens, M. McGuire, R. Jin, J. He, S. H. Curnoe, B. C. Sales, P. Blaha, D. J. Singh, K. Schwarz, and D. Mandrus, Phys. Rev. Lett. **92**, 065501 (2004).

[6] H. Sakai, K. Ikeura, M. S. Bahramy, N. Ogawa, D. Hashizume, J. Fujioka, Y. Tokura, and S. Ishiwata, Sci. Adv. **2**, e1601378 (2016).

[7] V. Kozii and L. Fu, Phys. Rev. Lett. **115**, 207002 (2015).

[8] Y. Shi, Y. Guo, Xia Wang, A. J. Princep, D. Khalyavin, P. Manuel, Y. Michiue, A. Sato, K. Tsuda, S. Yu *et al.*, Nat. Mater. **12**, 1024 (2013).

[9] N. V. Sidgwick, *The Electronic Theory of Valency* (Oxford University Press, UK, 1927).

[10] L. Shimoni-Livny, J. P. Glusker, and C. W. Bock, Inorg. Chem. **37**, 1853 (1998).

[11] S. A. J. Kimber, J. A. Rodgers, H. Wu, C. A. Murray, D. N. Argyriou, A. N. Fitch, D. I. Khomskii, and J. P. Attfield, Phys. Rev. Lett. **102**, 046409 (2009).

[12] J. G. Cheng, J. S. Zhou, and J. B. Goodenough, Phys. Rev. B **80**, 174426 (2009).

[13] J. B. Goodenough and J. Zhou, Sci. Technol. Adv. Mater. **16**, 036003 (2015).

[14] S. Hayashi and R. Aoki, Mater. Res. Bull. **14**, 409 (1979).

[15] J. Rodriguez-Carvajal, Physica B **192**, 55 (1993).

[16] F. Izumi and K. Momma, Solid State Phenom. **130**, 15 (2007).

[17] See Supplemental Material at http://link.aps.org/supplemental/10.1103/PhysRevB.95.155105 for the powder XRD data of Pb$_{1-x}$Sr$_x$MoO$_3$, the detailed structure analysis for the neutron diffraction data, and the analysis of the specific heat and magnetic susceptibility of PbMoO$_3$.

[18] D. A. Keen and A. L. Goodwin, Nature (London) **521**, 303 (2015).

[19] G. Burns and F. H. Dacol, Solid State Commun. **48**, 853 (1983).

[20] S. B. Vakhrushev, B. E. Kvyatkovsky, A. A. Naberezhnov, N. M. Okuneva, and B. P. Toperverg, Ferroelectrics **90**, 173 (1989).

[21] K. Hirota, Z. G. Ye, S. Wakimoto, P. M. Gehring, and G. Shirane, Phys. Rev. B **65**, 104105 (2002).

[22] R. B. Macquart, B. J. Kennedy, and M. Avdeev, J. Solid State Chem. **183**, 250 (2010).

[23] A. P. Ramirez and G. R. Kowach, Phys. Rev. Lett. **80**, 4903 (1998).

[24] T. H. K. Barron and G. K. White, *Heat Capacity and Thermal Expansion at Low Temperatures* (Springer, New York, 1999).

[25] R. O. Pohl and E. T. Swartz, J. Non-Cryst. Solids **76**, 117 (1985).

[26] D. J. Safarik, R. B. Schwarz, and M. F. Hundley, Phys. Rev. Lett. **96**, 195902 (2006).

[27] B. C. Melot, R. Tackett, J. O'Brien, A. L. Hector, G. Lawes, R. Seshadri, and A. P. Ramirez, Phys. Rev. B **79**, 224111 (2009).

[28] S. I. Ikeda and N. Shirakawa, Physica C **341**, 785 (2000).

[29] I. Nagai, N. Shirakawa, S.-i. Ikeda, R. Iwasaki, H. Nishimura, and M. Kosaka, Appl. Phys. Lett. **87**, 024105 (2005).

[30] H. Kronmüller and S. Parkin, *Handbook of Magnetism and Advanced Magnetic Materials* (Wiley-Interscience, New York, 2007).

[31] J. M. Ziman, *Electrons and Phonons* (Oxford University Press, New York, 1960).

[32] P. B. Allen and W. W. Schulz, Phys. Rev. B **47**, 14434 (1993).

[33] A. P. Mackenzie and Y. Maeno, Rev. Mod. Phys. **75**, 657 (2003).

[34] K. Kadowaki and S. B. Woods, Solid State Commun. **58**, 507 (1986).

[35] T. Masui, K. Yoshida, S. Lee, A. Yamamoto, and S. Tajima, Phys. Rev. B **65**, 214513 (2002).

[36] A. J. Millis, R. Mueller, and B. I. Shraiman, Phys. Rev. B **54**, 5389 (1996).

[37] H. F. Zhao, L. P. Cao, Y. J. Song, S. M. Feng, X. Shen, X. D. Ni, Y. Yao, Y. G. Wang, R. M. Wang, C. Q. Jin *et al.*, J. Solid State Chem. **246**, 92 (2017).